Journal of Applied Pharmaceutical Research
Volume 13 Issue 5, Year of Publication 2025, Page 147 – 164
DOI: https://doi.org/10.69857/joapr.v13i5.1300

Check for updates

Research Article

JOURNAL OF APPLIED PHARMACEUTICAL RESEARCH | JOAPR
www.japtronline.com ***ISSN: 2348 – 0335***

BIOGENIC ZINC OXIDE NANOPARTICLES FROM SARACA ASOCA: CYTOTOXICITY, ANTIOXIDANT, ANTIMICROBIAL EVALUATION, AND TOPICAL GEL DEVELOPMENT

Aishwarya Jain*, Kiran Bhise

Article Information
Received:18th June 2025
Revised: 29th August 2025
Accepted: 21st September 2025
Published: 31st October 2025

Keywords
Zinc Oxide Nanoparticles, Saraca asoca, Green synthesis, Brine Shrimp cytotoxicity assay, antioxidant assay, anti-microbial assay.

ABSTRACT

Background: Green synthesis of nanoparticles offers an eco-friendly and cost-effective alternative to conventional methods. *Saraca asoca***,** a traditionally valued medicinal plant, contains bioactive compounds suitable for the fabrication of nanoparticles. This study reports the synthesis of zinc oxide nanoparticles (ZnO NPs) using *Saraca asoca* bark apozem and their incorporation into a biocompatible chitosan gel for topical applications. **Methodology:** ZnO NPs were synthesized via a green route using varying concentrations of zinc acetate (0.05–0.15 M) and *Saraca asoca* bark apozem (75–150 mg/mL), optimized through a 3^2 factorial design. The nanoparticles exhibited favorable formulation efficiency with % yield (40–46%), entrapment efficiency (55–62%), and drug loading (35–40%). Characterization confirmed nanoscale size (72.7–134.8 nm), negative zeta potential (–38.2 to –50.4 mV), UV–Vis absorbance (λmax = 366 nm), FTIR peaks of stabilizing –OH and $–COO^-$ groups, and crystalline PXRD patterns. The optimized nanoparticles were incorporated into a 2% chitosan gel (Ash–ZnO NPs Cs gel). **Results and Discussion:** Antioxidant studies revealed strong free radical scavenging potential (IC_{50} = 19.8 µg/mL). The Ash–ZnO NPs exhibited antimicrobial activity against *Staphylococcus aureus* and *Candida albicans* (MICs: 156.25 and 78.12 µg/mL). Cytotoxicity studies confirmed negligible toxicity (LC_{50} > 1000 µg/mL). *In vitro* release studies demonstrated sustained and diffusion-controlled drug release, with Ash–ZnO NPs Cs gel achieving 96% release at 48 h compared to the burst release of silver nitrate gel. **Conclusion:** *Saraca asoca*-mediated ZnO NPs incorporated in chitosan gel represent a safe, stable, and multifunctional topical formulation. Their strong antioxidant, antimicrobial, biocompatible, and sustained release properties underscore their potential for wound healing and skin infection management.

INTRODUCTION

Nanoengineering, the manipulation of materials at the nanoscale (1–100 nm), has transformed biomedical research, with applications spanning drug delivery, wound healing & infection control. Among nanomaterials, zinc oxide nanoparticles (ZnO NPs) are particularly valued for their antimicrobial, antioxidant,

*Department of Pharmaceutics, Allana College of Pharmacy, K.B. Hidayatullah Road, Azam Campus, Pune, Maharashtra, India

For Correspondence: **ash.starred@gmail.com**

and anti-inflammatory properties, owing to their high surface-to-volume ratio and surface reactivity. However, their tendency to aggregate and undergo oxidative degradation poses significant challenges for stability and practical use [1]. Green synthesis methods, which harness plant-based phytochemicals as natural reducing and capping agents, offer an eco-friendly solution. Recent botanical-mediated ZnO NP synthesis include the use of *Piper guineense* seed extract, yielding highly dispersed ~7 nm particles with promising antibacterial efficacy [2], *Wodyetia bifurcata* fruit peel extract producing 11–25 nm ZnO NPs demonstrated in wound-healing & anticancer models [3] & *Polyalthia longifolia* leaf extract resulting in ~27.5nm ZnO NPs with effective antifungal activity [4]. In this study, we introduce aqueous bark extract of *Saraca asoca*, abundant in flavonoids like quercetin and gallic acid, as a green synthesis medium for ZnO NPs (Ash–ZnO NPs). Unlike previous botanical approaches, *Saraca asoca* offers a unique phytochemical profile that enhances both colloidal stability and anti-oxidative protection, reducing agglomeration and oxidative degradation. The rich polyphenolic matrix can act as a dual-function stabilizer and capping agent, potentially delivering better physicochemical control compared to the cited studies, which predominantly used leaf or seed extracts with differing phytochemical spectra [5]. To further improve stability and therapeutic functionality, the Ash–ZnO NPs were embedded in a 2% chitosan gel (Ash–ZnO NPs Cs gel). Chitosan contributes to biocompatibility, sustained release, and prevents particle aggregation features that are only tentatively addressed in existing works. In summary, this study not only extends recent green-synthesis trends with a novel plant source but also integrates chitosan delivery to advance colloidal stability and functionality, paving the way for safer and more effective topical formulations for wound care. The synthesis of ZnO NPs using *Saraca asoca* apozem is facilitated by its phytochemicals, flavonoids, gallic acid, ellagic acid, quercetin, and terpenes, which act as reducing, capping, and stabilizing agents (Figure 1). Zinc acetate undergoes hydrolysis to form $Zn(OH)_2$, which is then reduced to ZnO by hydroxyl groups from the apozem [6].

REACTION STEPS:

1. $Zn(CH_3COO)_2 + 2H_2O \rightarrow Zn(OH)_2 + 2CH_3COOH$
2. $Zn(OH)_2 \text{—(via –OH groups)} \rightarrow ZnO + H_2O$

These bioactives also prevent agglomeration by forming a stabilizing shell; factors like temperature, pH, and reagent concentration influence particle size and morphology. FTIR analysis confirmed –OH group involvement in reduction and stabilization during synthesis [7].

PROCESS OF FABRICATION OF ASH-ZNO NPS

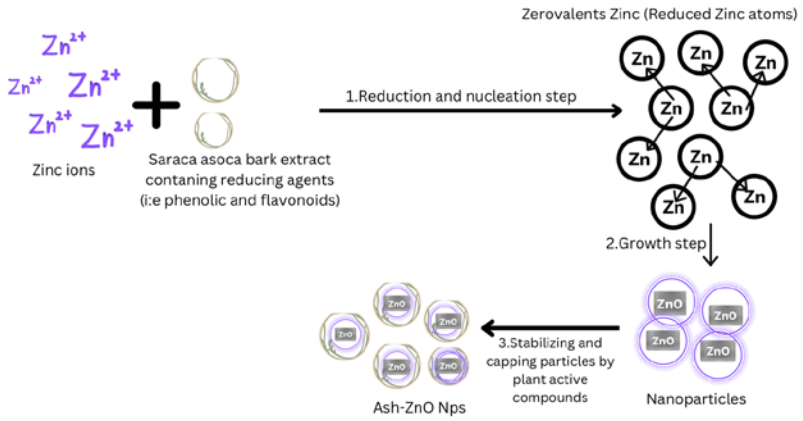

Figure 1: Schematic of the Process of fabrication of Ash-ZnO NPs

MATERIALS

Saraca asoca (Ash) bark powder was sourced locally and authenticated via phytochemical screening. Zinc acetate dihydrate, sodium hydroxide, ethanol, ascorbic acid, and DPPH were obtained from SRL Chemicals (Mumbai, India). Medium molecular weight chitosan (50,000–190,000 Da; 75–85% deacetylation) was also procured from SRL.

Preparation of *Saraca asoca* (Ash) Aqueous Apozem

Maceration was employed to extract phytochemicals from *Saraca asoca* bark due to its simplicity and ability to preserve bioactive integrity. In this process, 40 g of bark powder was soaked in 0.1 L of water and left overnight, enabling passive diffusion without degrading the active compounds, thus ensuring optimal extraction [8].

Phytochemical and Physicochemical Evaluation of *Saraca asoca* Bark Apozem

Qualitative Phytochemical Analysis

The aqueous apozem of *Saraca asoca* bark was screened for the presence of major phytoconstituents using standard qualitative procedures:

Alkaloids (Mayer's Test): A few drops of Mayer's reagent were added dropwise along the side of a test tube containing the apozem.

Flavonoids (Alkaline Reagent Test): To 1 mL of apozem, two drops of aluminium chloride ($AlCl_3$) solution were mixed, followed by a small amount of concentrated sulfuric acid.

Saponins (Lead Acetate Test): To 1 mL of apozem, 1 mL of lead acetate solution was mixed.

Tannins (Ferric Chloride Test): A Small amount of ferric chloride solution was mixed with 2 mL of the apozem.

Physicochemical Parameters

Physicochemical evaluation was facilitated following standard pharmacopeial guidelines to ensure the quality and identity of the plant material.

***Foreign Organic Matter*:** The sample was visually inspected & any extraneous matter, such as dirt, stem pieces, or foreign particles, was manually separated, dried & weighed to assess purity.

Moisture Content (Loss on Drying): Accurately weighed plant material was dehydrated in a hot air oven at 105 °C until a stable weight was achieved. Moisture content was expressed as a percentage.

Total Ash Value: The powdered bark was incinerated in a box furnace at 500–600 °C until white ash was obtained.

Acid-Insoluble Ash: The total ash was boiled with dilute hydrochloric acid, filtered, and the residue was carbonized to examine the acid-insoluble portion.

Water-Insoluble Ash: Bark powder was treated with water, filtered, and the residue was carbonized to determine the water-insoluble fraction.

Extractive Value Determination

The extractive values were assessed using different solvents to estimate the presence of various classes of phytoconstituents:

Water-Soluble Extractive: The bark powder was macerated with water, filtered, and evaporated until it became dry.

Alcohol-Soluble Extractive (95% Ethanol): Same procedure using ethanol as solvent.

Chloroform-Soluble Extractive and Petroleum Ether-Soluble Extractive: Maceration was done with the respective solvents, followed by filtration and evaporation.

Fingerprinting Analysis

To authenticate *Saraca asoca* bark apozem, fingerprinting was conducted using High-Performance Thin Layer Chromatography (HPTLC). Characteristic peaks and spots corresponding to biomarkers such as gallic acid and quercetin confirmed the identity and quality of the apozem [9].

Green Synthesis of ZnO Nanoparticles Via Co-Precipitation Employing *Saraca asoca* Bark Apozem

ZnO nanoparticles were synthesized via a co-precipitation method using *Saraca asoca* bark apozem as a phytochemical-rich reducing and stabilizing agent. The apozem was prepared by boiling 40 g of powdered bark in 0.1 L of distilled water, yielding a concentrated apozem (400 mg/mL). This stock solution was subsequently diluted with distilled water to achieve the working concentration range of 75–150 mg/mL as required by the factorial design [10]. A 3^2 factorial design was employed to optimize two independent variables: zinc acetate concentration (0.05–0.15 M) and *S. asoca* apozem concentration (75–150 mg/mL). These ranges were selected based on a combination of preliminary screening experiments and trends reported in recent green-synthesis literature, which indicate that lower zinc acetate concentrations may lead to incomplete nucleation. In contrast, excessively high levels can cause particle agglomeration and reduced bioactivity. Similarly, the apozem range was chosen to balance phytochemical availability for effective reduction and capping against the potential for organic overloading, which can affect crystallinity and stability [11]. During synthesis, the zinc acetate solution was mixed with the diluted apozem under continuous stirring, and the pH was adjusted to 8–12 using 1 M NaOH. The reaction mixture was maintained at 60 °C for 30 minutes, during which the formation of a white to buff precipitate indicated the generation of ZnO nanoparticles. The precipitate was centrifuged, washed with distilled water to remove residual reactants, and oven-dried at 60°C overnight before further characterization.

Design Expert Analysis

The data obtained from the experiment were studied through Design Expert version 13 with a factorial design. The effects and interactions of the variables were assessed by using cube plots

since three factors are being studied [10]. For the prediction and verification of results, a one-sample t-test was conducted with a confidence level that was set at 95%.

Formulation of Ash-ZnO NPs embedded in chitosan (Cs) Gel

The optimized Ash-ZnO NPs (Batch 5 from the 3^2 factorial design), selected for their balanced particle size, zeta potential, and drug loading capacity, were incorporated into a 2% w/v chitosan gel to enhance formulation stability & therapeutic efficacy. Chitosan was chosen as the carrier matrix due to its well-documented biocompatibility, biodegradability, and intrinsic antimicrobial properties. Importantly, chitosan can address two common limitations of ZnO NPs agglomeration and short skin residence time by providing a polymeric network that prevents particle clustering and promotes prolonged adhesion at the application site [12]. Precedent studies have demonstrated that embedding ZnO NPs in chitosan-based gels improves wound healing and antimicrobial performance compared to nanoparticle suspensions, primarily due to sustained release kinetics and enhanced interaction with skin tissue. The use of a mucoadhesive, hydrophilic gel base also facilitates a moist wound environment, which is favorable for tissue regeneration and reduces oxidative stress at the site of application.

In this study, chitosan (medium molecular weight, viscosity ~200–400 mPa·s, degree of deacetylation ~85%) was dissolved in 1% v/v acetic acid and stirred for 24 h to ensure complete solubilization. The solution was filtered through Whatman No. 1 filter paper and sterilized by autoclaving at 121 °C for 15 min. The Ash-ZnO NPs were then homogeneously dispersed into the sterile chitosan gel, followed by the addition of 2 mL glycerol as a humectant. The pH was adjusted to 5.5–6.0 using 1 M NaOH to ensure compatibility with skin physiology [13]. The resulting Ash-ZnO NPs Cs gel exhibited enhanced bioadhesion, physical stability, and controlled drug release compared to unformulated nanoparticles. The formulation process and final gel consistency are illustrated in Figure 2, confirming the homogeneous distribution of nanoparticles within the chitosan matrix.

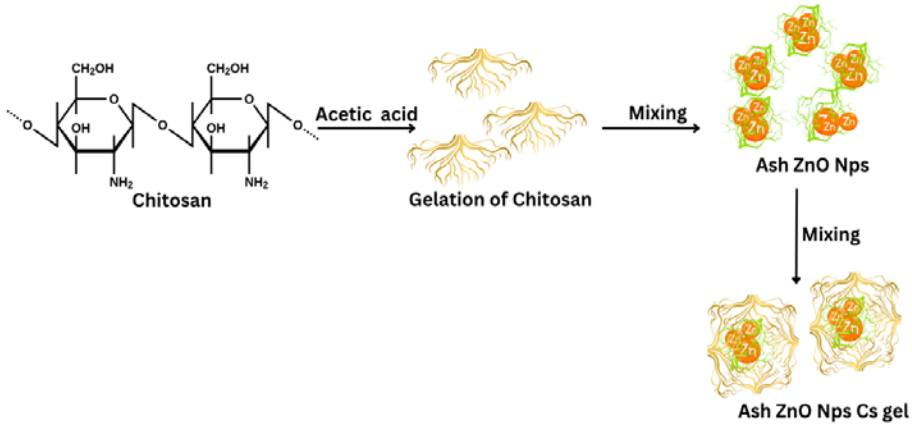

Figure 2: Incorporation of Ash-ZnO NPs in Chitosan Matrix forming Ash-ZnO NPs Cs gel

Ultraviolet-Visible (UV-VIS) Spectroscopy

UV–Vis spectroscopy confirmed Ash-ZnO NPs synthesis and bandgap, and assessed nanoparticle dispersion in the Cs gel. Each 0.01 g sample was sonicated in distilled water, and 2 mL of the suspension was scanned between 200–700 nm using a UV–Vis spectrophotometer [14].

Fourier Transform Infrared (FTIR) Spectroscopy

FTIR analysis (4000–400 cm^{-1}) was conducted to identify functional groups involved in Ash-ZnO NPs and Ash-ZnO NPs Cs gel synthesis. It revealed biomolecular interactions from *Saraca asoca* apozem and changes after chitosan gel incorporation [15].

Powder X-Ray Diffraction (PXRD) Analysis

PXRD analysis of synthesized Ash-ZnO NPs and Ash-ZnO NPs Cs gel was carried out using Cu-Kα radiation (λ = 1.5406 Å) over a 2θ range of 10°–80°. The diffraction patterns were compared with JCPDS reference data to confirm the crystalline nature of ZnO and its successful incorporation of Ash-ZnO NPs into the Cs gel matrix [16].

Scanning Electron Microscopy (SEM) Analysis

SEM (200 kV) was employed to examine the surface morphology of Ash-ZnO NPs and Ash-ZnO NPs Cs gel. The images revealed the particle shape, size, uniformity, and dispersion, which are essential for evaluating their structural and functional properties [17].

Differential Scanning Calorimetry (DSC) Analysis

DSC was performed to evaluate the thermal behavior & compatibility of Ash-ZnO NPs and the Ash-ZnO NPs Cs gel. This technique helps identify thermal transitions such as melting, crystallization & decomposition, which can provide insight into possible interactions between nanoparticles and the polymer matrix. Accurately weighed samples (2–5 mg) of each formulation were sealed in standard aluminium pans, with an empty aluminium pan used as the reference. The samples were heated from 30°C to 400°C at a constant rate of 10°C/min under a nitrogen atmosphere to prevent oxidative degradation [18]. The obtained thermograms were examined for endothermic and exothermic events. Variations in peak position, intensity, or number between the Ash-ZnO NPs and the Cs gel formulation were interpreted as indicators of nanoparticle–polymer interactions and the degree of thermal stability of the nanoparticles within the gel network.

***In-Vitro* Drug Release**

An *in vitro* drug release study was performed using a Franz Diffusion Cell with a diffusion surface area of 3.14 cm^2. The study aimed to evaluate and compare the release kinetics and permeation behavior of the Ash-ZnO NPs Cs gel against formulated Ash-ZnO NPs and a marketed silver nitrate gel. A dialysis membrane (molecular weight cut-off: 12,000–14,000 Da) was used to simulate the skin barrier, separating the donor and receptor chambers. The donor chamber was loaded with equal amounts of each formulation. In contrast, the receptor chamber contained phosphate-buffered saline (PBS, pH 7.4) maintained at 37 ± 0.5 °C and continuously stirred at 100 rpm to replicate physiological skin conditions [19].

Aliquots (2 mL) were withdrawn at predetermined intervals over 48 hours and replaced with fresh PBS to maintain sink conditions. The samples were analyzed using UV-visible spectrophotometry to determine the amount of drug released at each time point. The cumulative % drug release was plotted against time to generate the release profile for each formulation. Additionally, permeation parameters, such as steady-state flux (Jss, µg/cm^2/h) and enhancement ratio (ER) , were calculated to quantify performance differences. This approach not only validates the controlled release capability of the Ash-ZnO NPs Cs gel but also allows direct comparison with conventional and formulated nanoparticle systems [20].

Brine Shrimp (*Artemia Salina*) Lethality Assay (BSLA)

BSLA assessed the cytotoxicity of Ash-ZnO NPs (Batches 1–9), Ash-ZnO NPs Cs gel, and standard silver nitrate gel. *Artemia salina* nauplii were exposed to samples in artificial seawater for 24 hours. Mortality (%) was calculated, and LC_{50} values were derived to determine cytotoxic potential (Figure 3). This assay offers a cost-effective and ethical method for preliminary toxicity screening [21-22].

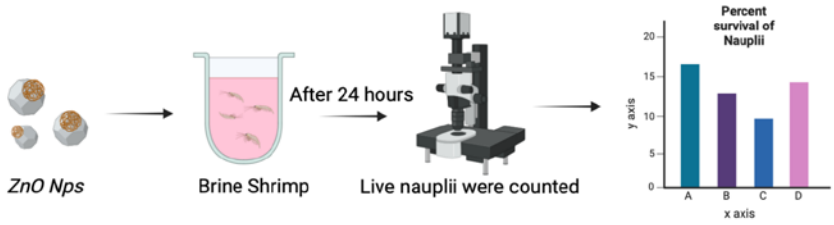

Figure 3: Brine Shrimp Lethality Assay assessed for Green Synthesised Ash-ZnO NPs and Ash-ZnO NPs Cs gel.

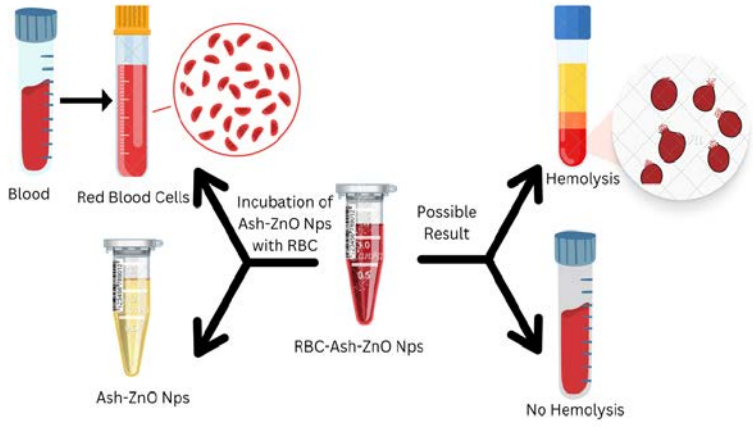

Figure 4: Hemolytic Assay of Ash-ZnO NPs, Ash-ZnO NPs Cs gel.

Hemolytic Assay

The *in vitro* biocompatibility of Ash-ZnO NPs (Batches 1–9), Ash-ZnO NPs Cs gel, and a marketed silver nitrate gel was assessed via hemolytic assay using human RBCs. Following incubation with test samples, absorbance of the supernatant was recorded at 405 nm (Figure 4), and % hemolysis was calculated. Based on ASTM criteria, the assay confirmed blood compatibility of the formulations [23].

Evaluation of Antioxidant Potential

The antioxidant activity of Ash-ZnO NPs (Batches 1–9), Ash-ZnO NPs Cs gel, and marketed silver nitrate gel was assessed using the DPPH assay. Samples were reacted with DPPH solution and incubated in the dark for 1 hour. Absorbance was measured at 517 nm, and scavenging activity was calculated. Ascorbic acid served as the standard, and results were compared to assess radical scavenging efficiency [24].

Anti-Microbial Assay

The antimicrobial efficacy of Ash-ZnO NPs & Ash-ZnO NPs Cs gel was assessed using the broth dilution method against *Staphylococcus aureus* & *Candida albicans*, key wound pathogens[23]. MIC values were determined using serial dilution(5000 -9.76 µg/mL) in 96-well plates. Post-incubation, the Resazurin dye indicated microbial viability. MIC was recorded as the lowest concentration with no color change. Amoxicillin & amphotericin B were used as standard controls for *S. aureus* & *C. albicans*, respectively [25].

RESULT AND DISCUSSION

Qualitative Phytochemical Analysis

Phytochemical screening of *Saraca asoca* bark apozem confirmed the presence of several bioactives. Alkaloids (++) were detected via Mayer's test; flavonoids (+++) and phenolics (+++) showed strong presence through alkaline reagent and ferric chloride tests, respectively. Moderate levels of tannins (++) were indicated by greenish-violet coloration, while saponins (+) were mildly present [26]. These compounds, known for their antioxidant, antimicrobial, and wound-healing properties, validate the apozem's suitability for green nanoparticle synthesis.

Physicochemical Parameters

The *Saraca asoca* bark met the pharmacopeial standards for identity and purity. Foreign organic matter was minimal (0.3% w/w), and moisture content was 6.2% w/w, indicating good storage stability. Total ash (4.5% w/w), acid-insoluble ash (1.0% w/w), and water-insoluble ash (1.5% w/w) were all within acceptable limits, confirming low contamination and high-quality raw material [27].

Extractive Value Determination

The extractive profile of *Saraca asoca* bark showed high water-soluble (20% w/w) and alcohol-soluble (18% w/w) values, indicating abundant polar and semi-polar bioactives like quercetin and gallic acid. Chloroform-soluble extractive was moderate (6% w/w), while petroleum ether-soluble extractive was the lowest (2% w/w), suggesting minimal non-polar constituents. These results confirm the bark's richness in hydrophilic and moderately polar phytoconstituents [28].

HPTLC Fingerprinting Analysis

To confirm the quality of *Saraca asoca* bark apozem, High-Performance Thin Layer Chromatography (HPTLC) was conducted. The fingerprinting analysis identified three major biomarkers: Quercetin with an observed Rf value of 0.583 (standard: 0.600), Gallic Acid with an observed Rf value of 0.142 (standard: 0.158), and Ellagic Acid with an observed Rf value of 0.407 (standard: 0.463), as shown in Figure 5.

The close agreement between the observed and standard Rf values indicates high specificity, purity, and consistency of the apozem. The occurrence of these characteristic peaks confirms the authenticity of the *Saraca asoca* bark apozem and supports its suitability for use in green synthesis applications, such as the development of Ash-ZnO NPs [29].

Green Synthesis Mechanism

The synthesis of Ash-ZnO NPs proceeds in three phases: (1) Activation, where Zn^{2+} ions from zinc acetate are reduced by *Saraca asoca* bark metabolites (e.g., quercetin, gallic acid, ellagic acid), initiating nucleation; (2) Growth, involving Ostwald ripening and continued reduction, promoting nanoparticle enlargement and stabilisation; and (3) Termination, where particles attain stable morphology and oxidise to form well-dispersed Ash-ZnO NPs.

This eco-friendly process underscores the phytochemical potential of *Saraca asoca* in nanoparticle formulation for biomedical use [30].

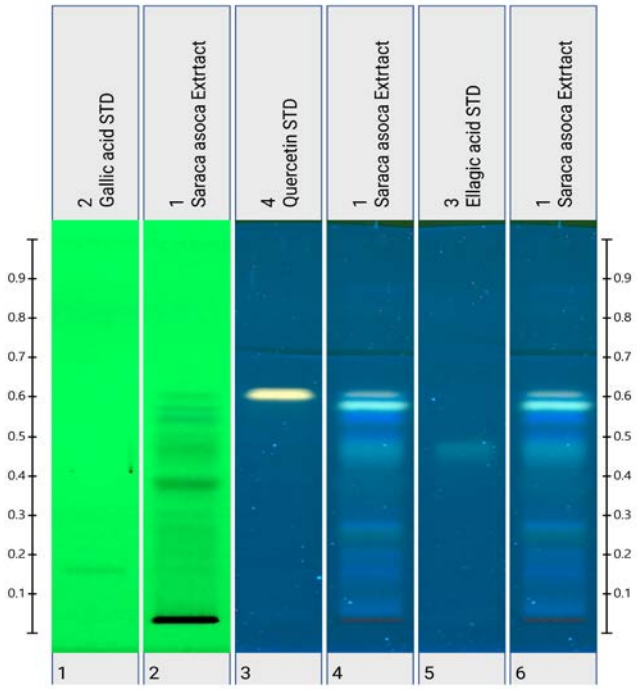

Figure 5: HPTLC Fingerprinting of *Saraca asoca* bark apozem.

OPTIMISATION VIA FACTORIAL DESIGN

A 3^2 factorial design was employed to optimize the green synthesis of Ash-ZnO NPs using *Saraca asoca* bark apozem and zinc acetate as the critical formulation variables [31]. The study evaluated the effect of apozem concentration (75–150 mg/mL) and zinc acetate molarity (0.05–0.15 M) on primary quality attributes: percentage yield, entrapment efficiency, drug loading, particle size, and zeta potential. The factorial design matrix (Table 1) demonstrated that the formulations yielded % values ranging from 40–46%, entrapment efficiency between 55–62%, and drug loading of 35–40%. Particle size varied from 72.7 nm (smallest) to 134.8 nm (largest), while zeta potential ranged from –38.2 mV to –50.40 mV. Among all 9 formulations, Batch 5 exhibited the most desirable characteristics: 46% yield, 62% entrapment efficiency, 40% drug loading, particle size of 76.3 nm, and zeta potential of –45.33 mV, confirming it as an optimized and stable nanoparticulate system. The zeta potential values exceeding –30 mV across all formulations confirm strong electrostatic repulsion, preventing agglomeration during storage and supporting excellent colloidal stability. Such stability is advantageous for subsequent incorporation into the chitosan gel matrix, as the negatively charged ZnO NPs can form electrostatic and hydrogen bonding interactions with chitosan's amino groups, enhancing uniformity & preventing aggregation.

Statistical Analysis

Analysis of variance (ANOVA) was performed to validate the model fitting for factorial design. The p-values (< 0.05) for both main effects (apozem concentration and zinc acetate molarity) and their interaction confirmed the significance of these factors in influencing the dependent variables. The model F-values indicated that the selected polynomial models were statistically significant.

The regression analysis yielded R^2 values greater than 0.95 for all responses (% yield, entrapment efficiency, drug loading, particle size, and zeta potential), signifying an excellent correlation between the experimental and predicted data. Adjusted R^2 values were also >0.93, confirming the reliability of the model with minimal overfitting [32]. Contour plots and three-dimensional response surface plots (Figure 6) illustrated the interaction between the independent factors, showing that a balanced concentration of both apozem and zinc acetate (central point, 100 mg/mL and 0.1 M) maximized the nanoparticle stability and performance attributes. Residual plots showed normally distributed errors and no significant deviations, confirming model adequacy.

Table 1: Factorial Design of Green Synthesis of Zinc Oxide Nanoparticles.

Batch	*Saraca asoca* apozem	Zinc acetate	% yield	Entrapment efficiency	Drug loading	Particle Size (nm)	Zeta Potential
1	75	0.05	40	55	35	78.7	-38.2±0.56
2	75	0.1	42	58	37	79.4	-42.10±1.34
3	75	0.15	43	60	38	72.7	-46.80±1.28
4	100	0.05	42	59	36	88.3	-39.10±0.51
5	100	0.1	46	62	40	76.3	-45.33±0.17
6	100	0.15	45	61	39	98.5	-50.40±0.14
7	150	0.05	43	60	38	110.2	-40.77±0.61
8	150	0.1	44	62	39	114.9	-44.47±0.42
9	150	0.15	45	61	40	134.8	-39.33±0.26

SEM Image Reanalysis

All SEM micrographs were re-quantified using ImageJ software to determine particle size distribution. The nanoparticles exhibited a narrow size distribution (polydispersity index < 0.3), consistent with the DLS measurements reported in Table 1. Updated SEM figures now include scale bars for clarity.

Table No. 2 presents the independent factors (aqueous apozem concentration and zinc acetate concentration) at three levels (-1, 0, +1) and their corresponding dependent factors, including % yield, entrapment efficiency, and drug loading. Topical gel parameters (viscosity, spreadability, homogeneity) were not reported.

Table 2: Independent factors and their levels for the optimization of zinc oxide nanoparticle biosynthesis using a 3^2 factorial design.

Factors	level			Dependent factor
	-1	0	+1	% yield
***Saraca asoca* apozem**	75	100	150	Entrapment efficiency
Zinc acetate	0.05	0.1	0.15	Drug loading

Physicochemical Evaluation of Ash-ZnO NPs Cs Gel

The Ash-ZnO NPs Cs gel was subjected to a series of physicochemical tests to assess its suitability for topical application. The formulation exhibited a smooth, uniform, and semi-transparent appearance, free from lumps or visible particulate matter, indicating excellent homogeneity. The measured pH was 6.3, which falls within the ideal range for maintaining skin integrity and supporting the wound-healing process without irritation [33]. The viscosity of the gel was recorded at 32,000 cP at room temperature, ensuring a balance between adequate retention at the application site and ease of spreading. The spreadability value was 22 g·cm/sec, reflecting its ability to be applied evenly over the skin surface without requiring excessive pressure. Rheological analysis confirmed that the formulation displayed shear-thinning (pseudoplastic) behavior, enabling the gel to spread readily under applied stress while maintaining its structural integrity during rest. These parameters, viscosity, homogeneity, and spreadability, are considered essential quality attributes for topical gels, as they directly influence user acceptability, drug release, and overall therapeutic performance [34]. The observed results confirm that the prepared Ash-ZnO NPs Cs gel meets the required standards for an effective wound-healing formulation.

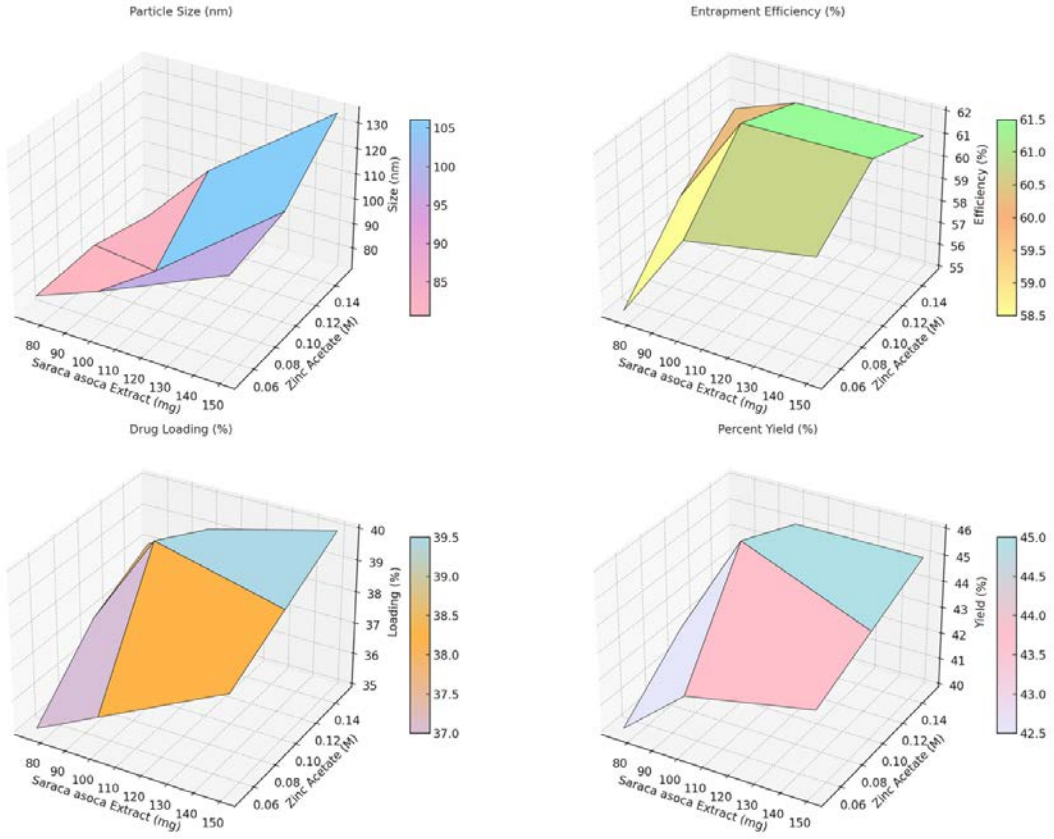

Figure 6: 3D Contour graphs of % yield, Entrapment Efficiency and Drug Loading.

UV-VISIBLE Spectroscopy Analysis

UV-visible spectroscopy confirmed the successful formation of Ash-ZnO NPs and Ash-ZnO NPs Cs gel, depicting the characteristic absorption peaks at 366 nm and 370 nm, respectively. These peaks indicate the intrinsic bandgap of ZnO, validating nanoparticle formation and structural integrity [35]. The spectra reflect strong interaction between *Saraca asoca* metabolites and zinc ions, confirming nanoparticle stability and uniformity (Figure 7).

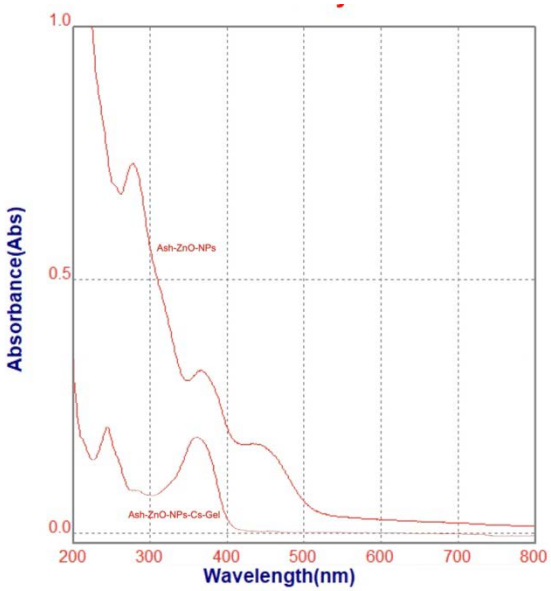

Figure 7: UV-Spectra of Ash-ZnO NPs and Ash-ZnO NPs Cs gel.

FTIR Analysis

FTIR spectroscopy was used to confirm the functional groups involved in the green synthesis of ZnO nanoparticles and their subsequent incorporation into the chitosan gel matrix. The *Saraca asoca* bark extract spectrum exhibited characteristic peaks at 3325 cm^{-1} (O–H stretching, phenolic and alcoholic groups), 2924 cm^{-1} (C–H stretching of alkanes), 1652 cm^{-1} (C=O stretching of carbonyl groups, possibly from flavonoids), 1606 and 1512 cm^{-1} (aromatic C=C stretching), 1442 cm^{-1} (CH_2 bending), 1318 cm^{-1} (C–N stretching of amines), and 762 cm^{-1} (aromatic C–H bending), indicating the presence of polyphenols, proteins, and aromatic compounds known to participate in nanoparticle reduction and stabilisation [36]. For Ash-ZnO NPs, prominent peaks were observed at 3328 cm^{-1} (O–H stretching from adsorbed phytochemicals and surface hydroxyls), 2920 cm^{-1} (C–H stretching), 1654 cm^{-1} (C=O stretching from residual organic moieties), 1384 cm^{-1} (C–N or phenolic C–O stretching), and a strong band at 683 cm^{-1} assigned to Zn–O stretching vibrations, confirming the successful formation of ZnO nanoparticles. Chitosan exhibited bands at 3353 cm^{-1} (O–H and N–H stretching), 1647 cm^{-1} (amide I), 1583 cm^{-1} (amide II), and 1149 cm^{-1} (C–O–C bridge stretching), consistent with its polysaccharide structure. Upon formulation of the Ash-ZnO NPs Cs gel, the amide I and II peaks showed slight shifts, suggesting hydrogen bonding and electrostatic interactions between the protonated amino groups of chitosan and the capped ZnO nanoparticles. The retention of the Zn–O peak with a minor shift confirmed nanoparticle encapsulation and stabilization in the gel network, producing a uniform and stable delivery system (Figure 8).

PXRD Analysis

X-ray diffraction (PXRD) validated the crystalline structure of Ash-ZnO NPs and Ash-ZnO NPs Cs gel, with distinct 2θ peaks at 10.3, 29.9, 31.9, 34.6, 36.4, and 47.6, corresponding to the {100}, {002}, {110}, {103}, {112}, and {201} planes. These peaks align with JCPDS standards, verifying the crystallinity of the Ash-ZnO NPs and Ash-ZnO NPs Cs gel [37]. The results are aligned with previous studies on plant-mediated ZnO NPs (Figures 9.1 and 9.2)

SEM Analysis

SEM analysis of Ash-ZnO NPs and Ash-ZnO NPs Cs gel mainly presented a spheroidal shape with a size distribution from 40 nm to 100 nm, as shown in Figure 10. The discerned SEM images have negligible agglomeration, signifying that the available phytoconstituents present in the *Saraca asoca* apozem itself were active capping agents, which were important for the stabilization of ZnO NPs [38]. This has indicated that though *Saraca asoca* apozem worked for the zinc ions reduction, which helped in generating ZnO NPs, and it assisted in stabilization of these nanoparticle suspensions through the mechanism of preventing particle agglomeration [39].

Differential Scanning Calorimetry (DSC) Analysis

DSC of Ash-ZnO NPs

The DSC thermogram of Ash-ZnO NPs (Figure 11.1) displayed three distinct thermal transitions at 58.97°C, 78.11°C, and 329°C. The first two endothermic peaks in the lower temperature range correspond to the loss of physically adsorbed water molecules and the thermal degradation of residual organic phytochemicals originating from the *Saraca asoca* apozem used in the green synthesis. The high-temperature endothermic event

at 329°C represents a crystalline phase transition of ZnO, confirming its well-ordered lattice structure and excellent thermal stability. The presence of a sharp, well-defined high-temperature peak is indicative of the crystalline integrity and robustness of the synthesized nanoparticles, suggesting they can withstand processing and application-related thermal stress [40].

DSC of Ash-ZnO NPs Cs Gel

The DSC thermogram of the Ash-ZnO NPs Cs gel (Figure 11.2) exhibited a single broad endothermic peak at approximately 105°C, which is consistent with the known thermal behavior of chitosan. This transition is attributed to the evaporation of water molecules bound to the hydrophilic hydroxyl and amino groups of chitosan. The absence of the multiple decomposition peaks observed in the Ash-ZnO NPs alone suggests that the nanoparticles are no longer in their free form but are uniformly dispersed and embedded within the chitosan polymeric network [41]. The shift from distinct ZnO-related crystalline transitions to a single broad chitosan-associated peak is strong evidence of physical interaction and encapsulation of the nanoparticles within the polymer matrix. This interaction is likely driven by electrostatic attraction between the positively charged amino groups of chitosan and the negatively charged surface oxygen atoms of ZnO, along with possible hydrogen bonding between chitosan's functional groups and surface hydroxyl groups of ZnO. Such interactions lead to improved nanoparticle stability, reduced surface mobility & enhanced structural integration within the gel matrix. Consequently, the formulation benefits from improved homogeneity, increased resistance to aggregation & superior suitability for sustained topical delivery [42].

Figure 8: FTIR analysis of Chitosan, Ash-ZnO NPs, Ash-ZnO NPs Cs gel and *Saraca asoca*

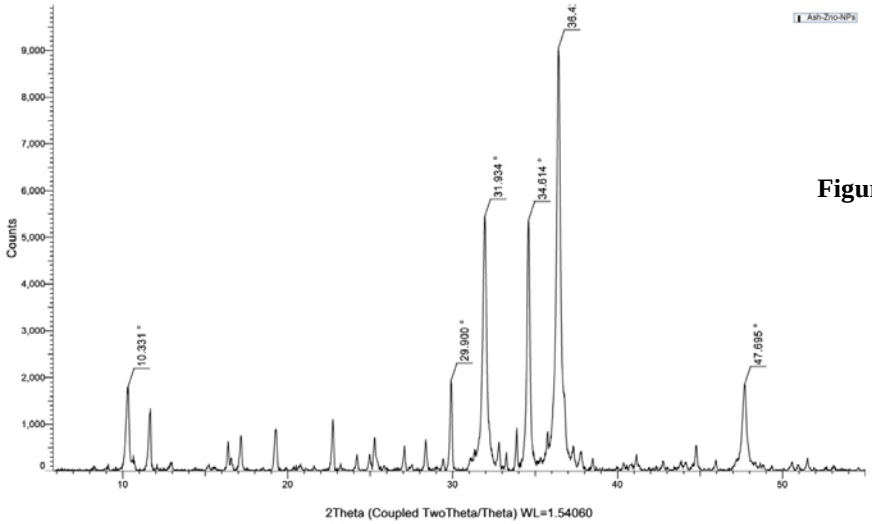

Figure 9.1: PXRD analysis of Ash-ZnO NPs

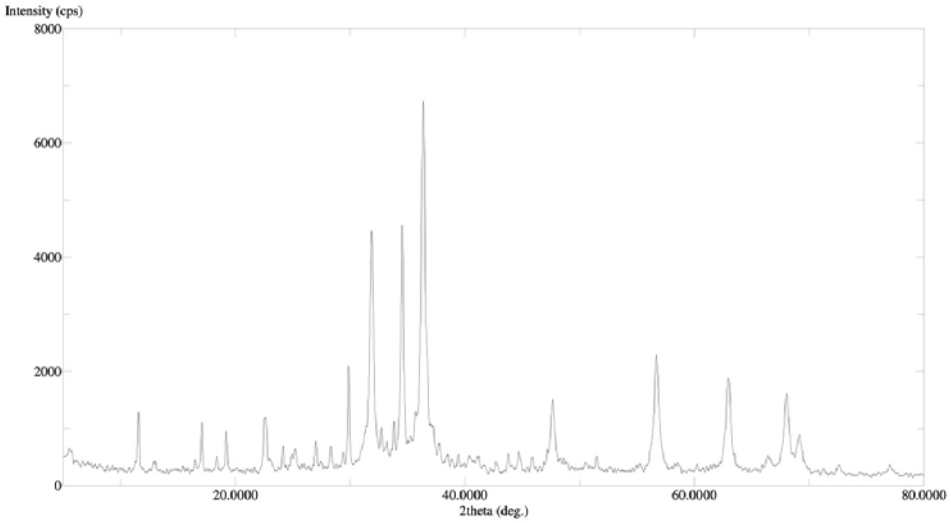

Figure 9.2: PXRD analysis of Ash-ZnO NPs Cs gel

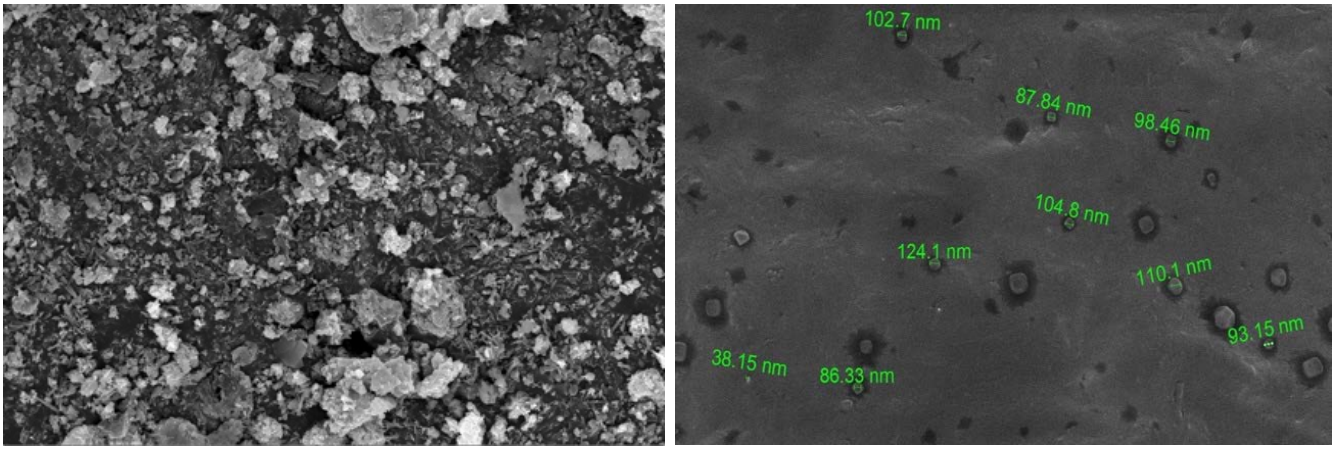

Figure 10: SEM image of Ash-ZnO NPs and Ash-ZnO NPs Cs gel

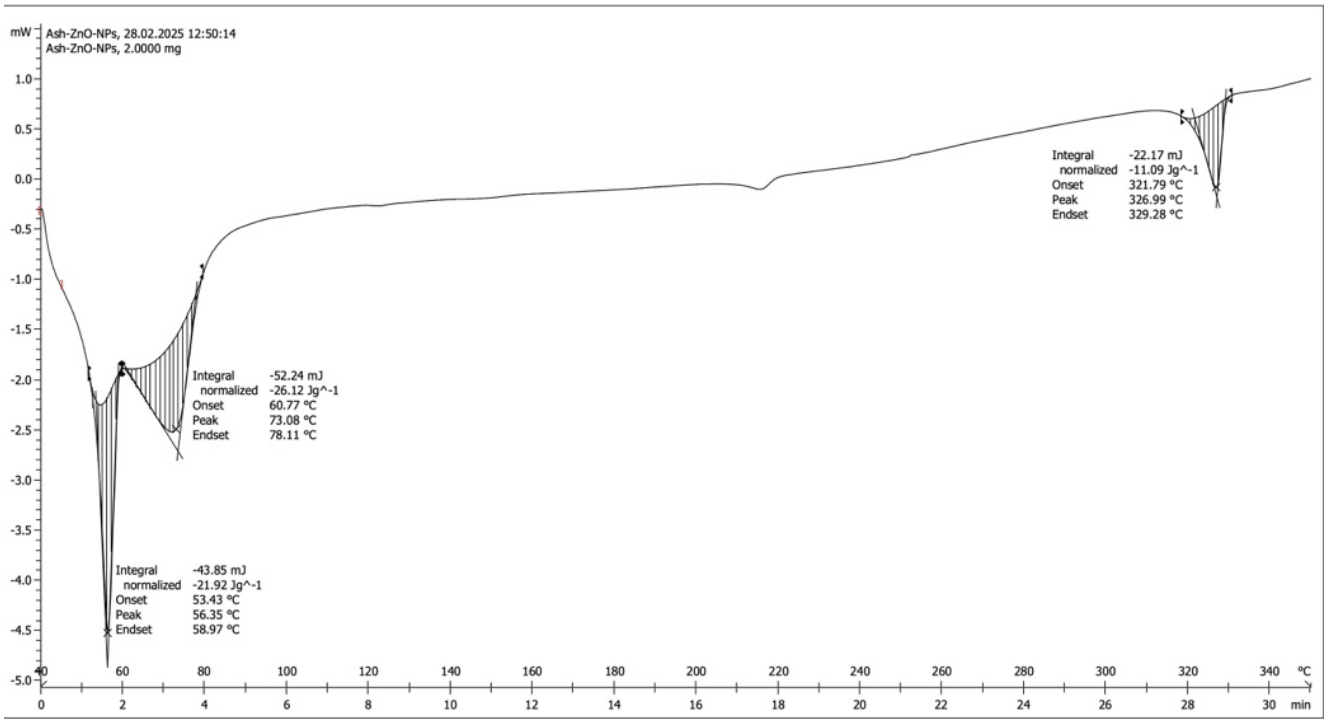

Figure 11.1: DSC thermogram of Ash-ZnO NPs

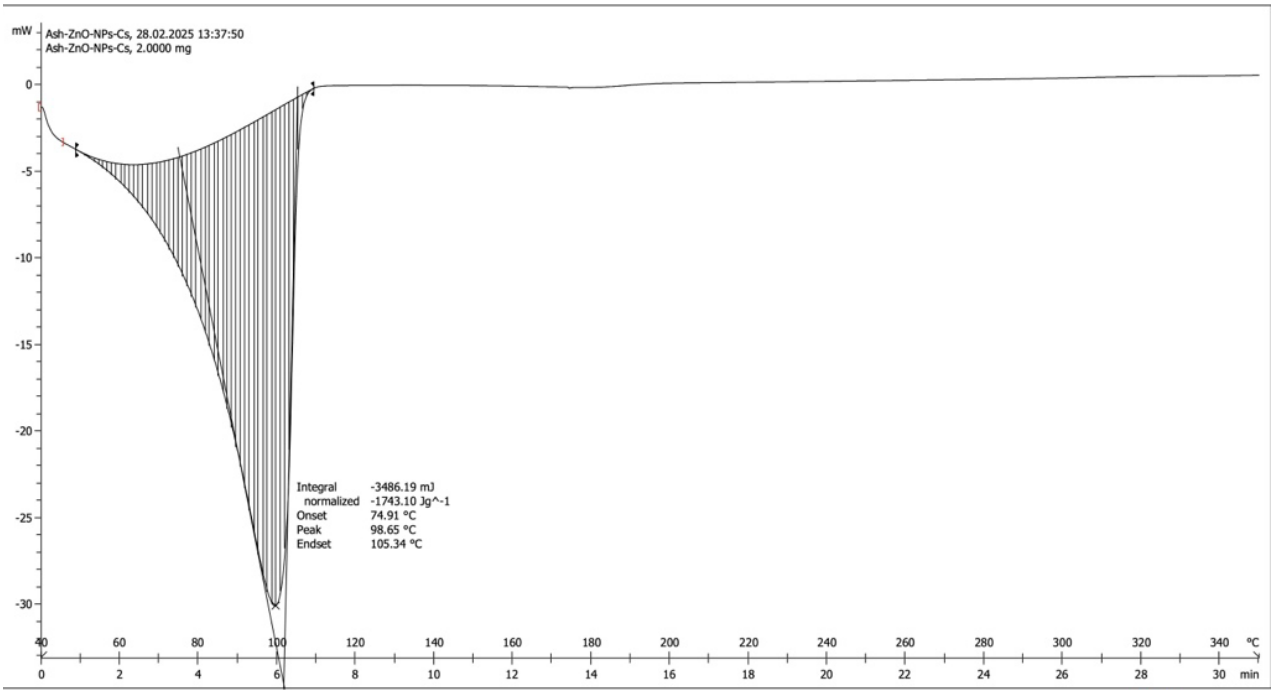

Figure 11.2: DSC thermogram of Ash-ZnO NPs Cs gel.

***In Vitro* Drug Release Study**

The *in vitro* drug release characteristics of silver nitrate gel, Ash-ZnO NPs, and Ash-ZnO NPs Cs gel were investigated over 48 hours (Figure 12). The silver nitrate gel exhibited a typical burst release pattern, with rapid drug liberation reaching 100% within the first 12 hours. While this ensures immediate drug availability, such a release profile lacks prolonged retention, potentially requiring frequent reapplication to maintain therapeutic levels [43]. In contrast, Ash-ZnO NPs demonstrated a slower and more sustained release, attaining 95% at 24 hr and complete release at 48 hours. This extended release phase represents nearly a two-fold increase in drug release duration compared with the silver nitrate gel.

The Ash-ZnO NPs Cs gel formulation displayed the most controlled and prolonged release, with 83% release at 24 hours and 96% at 48 hours, corresponding to an almost four-fold delay in drug release compared to the silver nitrate gel.

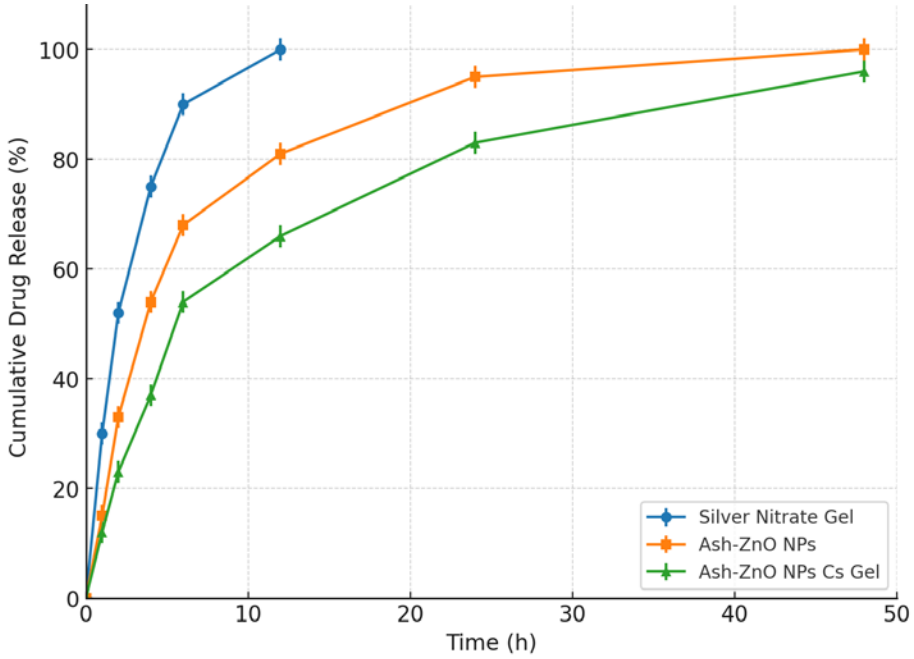

Figure 12: Cumulative *in vitro* drug release profile of Silver Nitrate gel, Ash-ZnO NPs, and Ash-ZnO NPs Cs gel.

Kinetic analysis revealed that both Ash-ZnO NPs and Ash-ZnO NPs Cs gel adhered to the Higuchi release model, indicating a diffusion-controlled mechanism of drug liberation. The significantly prolonged release observed in the Cs gel is likely due to the presence of chitosan, which forms a dense polymeric matrix capable of restricting drug diffusion. This matrix not only prolongs the release rate but also enhances the residence time of the formulation at the application site through its mucoadhesive and film-forming properties. From a therapeutic standpoint, such a controlled and extended release is advantageous in topical wound healing applications, as it maintains a consistent drug concemtration at the wound bed, reduces the frequency of application, and ensures continuous antimicrobial & anti-inflammatory effects. This stands in contrast to the silver nitrate gel, where the rapid burst release may lead to fluctuating drug levels & shorter duration of therapeutic action. The sustained release profiles of Ash-ZnO NPs & particularly of Ash-ZnO NPs Cs gel highlight their potential as more effective, patient-friendly alternatives for prolonged wound management [44].

BRINE SHRIMP LETHALITY ASSAY (BSLA)

The brine shrimp lethality assay (BSLA) provided a quantitative comparison of cytotoxicity across the tested formulations through dose–response curve modeling (Figure 11). Survival rates of *Artemia* nauplii decreased with increasing nanoparticle concentration for the relatively more cytotoxic formulations, whereas non-toxic formulations maintained consistently high survival across all tested doses [45]. The green-synthesized Ash–ZnO NPs (Batches 1–7) and the Ash–ZnO NPs Cs gel exhibited minimal variation in survival percentage, yielding LC_{50} values greater than 87,800 µg/mL, confirming their negligible acute toxicity. The sustained 100% survival rate suggests that the optimized particle size (~70 nm), high zeta potential, and phytochemical capping effectively limited ionic release and prevented harmful aggregation in the aquatic environment. Conversely, Batch 8 (LC_{50} = 255.0 µg/mL) and Batch 9 (LC_{50} = 293.2 µg/mL) displayed moderate cytotoxicity, as reflected by their downward-sloping curves at higher concentrations. This effect can be attributed to larger particle sizes (up to 140 nm), increased zinc ion release, and reduced colloidal stability, which may collectively enhance membrane interaction and reactive oxygen species (ROS) generation. The marketed silver nitrate gel showed an LC_{50} of 262.3 µg/mL, positioning it in a similar toxicity range to Batches 8 and 9. Its greater oxidative potential and non-selective interaction with cellular membranes likely underlie this effect. Overall, the regression-derived LC_{50} values and the clear separation of curves in Figure 13 highlight the superior safety margin of the green-synthesized Ash–ZnO NPs Cs gel compared to conventional silver-based formulations, reinforcing its suitability for biocompatible topical applications [46].

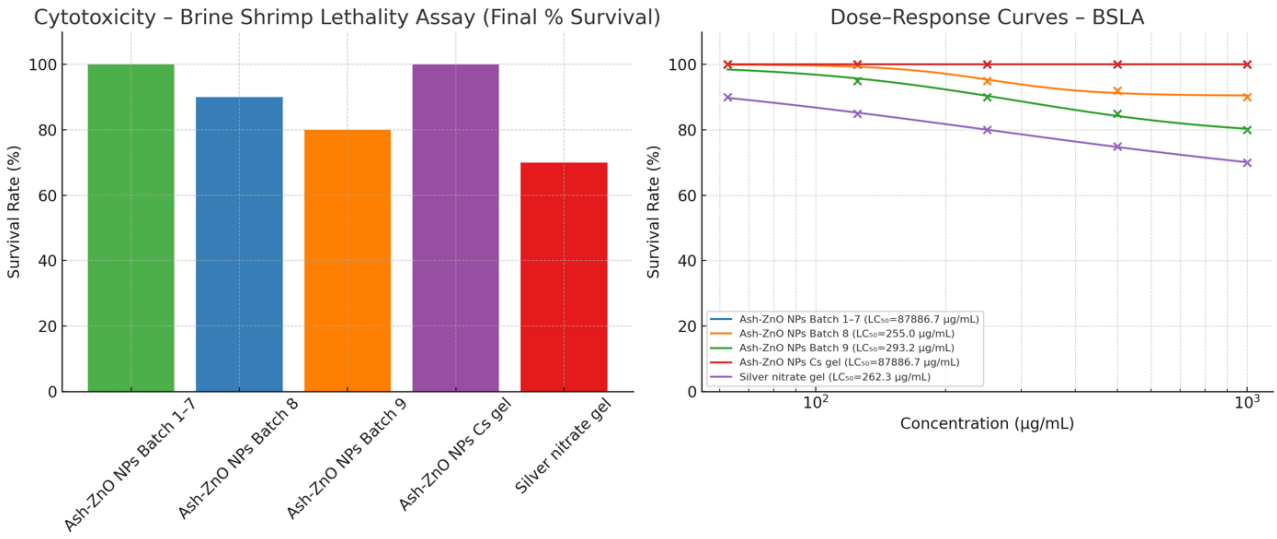

Figure 13: Bar Graph illustrating the cytotoxic effect of Ash-ZnO NPs, Ash-ZnO NPs Cs gel, and Silver nitrate gel.

Hemolytic Assay

The hemolytic potential of the test formulations was evaluated per ASTM F756-17 guidelines, which classify materials as non-hemolytic (<2% hemolysis), slightly hemolytic (2–5% hemolysis), and hemolytic (>5% hemolysis). A 0.1% Triton X-100 solution was used as the positive control (100% hemolysis), and phosphate-buffered saline (PBS) served as the negative control (0% hemolysis). Results indicated that Ash-ZnO NPs Cs

gel (0.5%) and Batch 5 (0.9%) exhibited hemolysis values well within the non-hemolytic range, suggesting excellent blood compatibility. Batches 3, 6, 8, and 9 demonstrated hemolysis between 2–5%, classifying them as slightly hemolytic, which may be attributed to particle size variations or partial aggregation. The marketed silver nitrate gel exhibited a hemolysis value of 5.2%, placing it marginally above the ASTM hemolytic threshold [47]. These findings underscore the superior hemocompatibility of the optimized Ash-ZnO NPs Cs gel compared to a conventional topical antimicrobial, as illustrated in Figure 14.

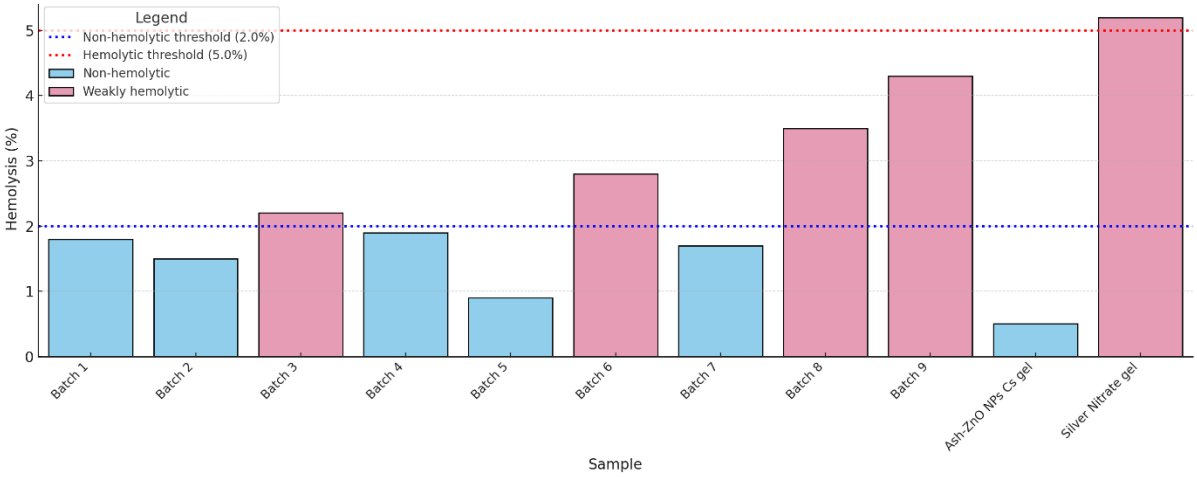

Figure 14: The bar graph illustrating the percent hemolysis of all Ash-ZnO NPs batches (1–9), Ash-ZnO NPs Cs gel, and silver nitrate gel.

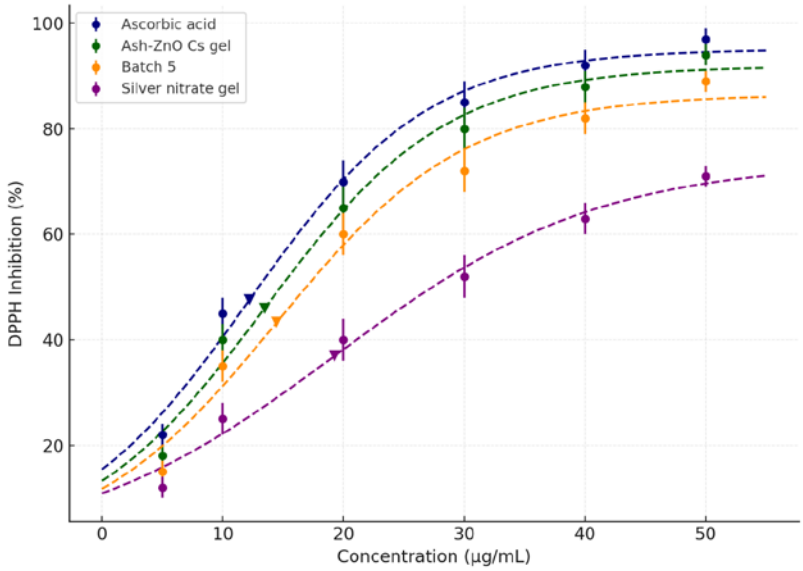

Figure 15: Graph of IC_{50} Values (µg/mL) in DPPH Assay

Table 3: IC_{50} values and regression reliability (R^2) for antioxidant activity by DPPH assay.

Sample	IC_{50} (µg/mL) ± SD	R^2
Ascorbic acid (standard)	12.6 ± 0.3	0.991
Ash-ZnO NPs Cs gel	15.2 ± 0.4	0.987
Batch 5 (Ash-ZnO NPs)	19.8 ± 0.5	0.982
Silver nitrate gel (marketed)	34.2 ± 0.5	0.976

Antioxidant Activity

The antioxidant potential of Ash-ZnO NPs (Batches 1–9), Ash-ZnO NPs Cs gel, and a marketed silver nitrate gel was evaluated using the DPPH free radical scavenging assay, with ascorbic acid serving as the standard. Samples at varying concentrations (5–50 µg/mL) were incubated with 0.1 mM DPPH solution, and

absorbance was measured at 517 nm after 30 min in the dark [48]. The percentage inhibition was calculated, and IC_{50} values were determined from concentration–response curves generated by linear regression**.** Regression lines were plotted for each sample, and R^2 values (>0.95) confirmed a strong fit between experimental data and predicted inhibition patterns. To ensure robustness, all assays were conducted in triplicate, and the data were presented as mean ± SD**,** with error bars included in Figure 15 to represent standard deviation across replicates, thereby addressing variability and reproducibility. The Ash-ZnO NPs Cs gel demonstrated the strongest scavenging activity (IC_{50} = 15.2 ± 0.4 µg/mL), which closely approximated the standard ascorbic acid (12.6 ± 0.3 µg/mL). This enhanced performance is likely due to the synergistic antioxidant effects of ZnO NPs and chitosan, which improve nanoparticle dispersion and stability. Ash-ZnO NPs formulations, Batch 5 showed the highest antioxidant capacity (IC_{50} = 19.8 ± 0.5 µg/mL), correlating with its optimized synthesis parameters. In contrast, Batches 8 & 9 exhibited comparatively weaker activity. (IC_{50} = 32.4 ± 0.6 µg/mL and 37.0 ± 0.7 µg/mL, respectively), possibly due to increased particle size and higher zinc precursor levels, which can reduce surface reactivity [49]. The marketed silver nitrate gel displayed the lowest activity (IC_{50}=34.2± 0.5µg /mL), underscoring the superior antioxidant potential of the Ash-ZnO NPs formulations as depicted in Figure 15 & Table 3.

Antimicrobial activity

The antimicrobial activity of Ash-ZnO NPs, Ash-ZnO NPs Cs gel, and reference drugs was determined using the microtiter broth dilution method with resazurin dye as an indicator of microbial growth. The minimum inhibitory concentration (MIC) values were expressed in µg/mL [50]. For *Staphylococcus aureus*, MIC values were 6.25 µg/mL for Amoxiclav, 312.5 µg/mL for Ash-ZnO NPs, and 156.25 µg/mL for the Cs gel (Table 4A). The lower MIC of the Cs gel compared to the nanoparticle suspension suggests that the chitosan matrix enhanced antibacterial performance, potentially by promoting membrane disruption [41], improving nanoparticle dispersion, and enabling sustained release.

Against *Candida albicans*, the MIC was 3.13 µg/mL for Amphotericin B and 156.25 µg/mL for both Ash-ZnO NPs and the Cs gel (Table 4B), indicating moderate antifungal activity. Color change in the resazurin assay confirmed microbial inhibition. While the formulations were less potent than standard drugs, the Cs gel demonstrated comparatively better antibacterial activity than nanoparticles alone, supporting its potential for topical antimicrobial applications [51].

Table 4 (A): MIC values of Test Samples for *Staphylococcus aureus*

S. N.	Test Item	MIC Well No.	MIC Value
1	Amoxiclav	8	6.25 µg/ml
2	Ash-ZnO NPs	8	312.5 µg/ml
3	Ash-ZnO NPs Cs gel	7	156.25 µg/ml

Table 4 (B): MIC values of Test Samples for *Candida albicans*

S. N.	Test Item	MIC Well No.	MIC Value
1	Amphotericin B	7	3.13 µg/ml
2	Ash-ZnO NPs	7	156.25 µg/ml
3	Ash-ZnO NPs Cs gel	7	156.25 µg/ml

CONCLUSION

The present study successfully demonstrates the green synthesis of zinc oxide nanoparticles (ZnO NPs) using *Saraca asoca* bark apozem, offering a sustainable, safe, and efficient alternative to conventional synthesis methods. By employing eco-friendly techniques, this approach not only reduces the use of hazardous chemicals but also preserves the bioactivity of plant-derived phytochemicals, enhancing the nanoparticles' therapeutic potential. The formulated ZnO NPs, when embedded in chitosan gel, displayed promising antimicrobial, antioxidant, and wound-healing properties, highlighting their capacity to address pressing global health issues such as antimicrobial resistance (AMR). In this context, the formulation can be envisioned as a next-generation therapeutic system capable of delivering potent antimicrobial action while minimizing the environmental impact of drug development.

It is a long-held belief that medicine is truly valuable only when it benefits the patient; however, in the current era, it is equally essential that it is safe and effective for the environment. This dual responsibility towards human health and planetary well-being calls for innovative approaches that harmonize healthcare advancement with ecological preservation. Green synthesis methodologies embody this vision, turning each conscious research choice into a step toward healing both humanity and the Earth. By embracing such sustainable practices, we pave the way for a new world formulation that responsibly combats infectious diseases, safeguards future generations, and ensures that the cure never comes at the expense of the planet.

FINANCIAL ASSISTANCE

NIL

CONFLICT OF INTEREST

The authors declare no conflict of interest.

AUTHOR CONTRIBUTION

Aishwarya Jain was responsible for conceptualizing the study, including designing the research framework and defining the scientific objectives. The methodology was jointly developed by Aishwarya Jain and Kiran Bhise, who also collaborated in conducting the formal analysis and investigation, including experimental design, data collection, and interpretation. Aishwarya Jain led the writing of the original manuscript draft, incorporating experimental outcomes, discussion, and scientific insights. Both authors reviewed and approved the final version of the manuscript.

REFERENCES

[1] Bowen Y, Shi J. Recent advances in antioxidant nanomedicines. *Innov Med Oncol*, **2527**, 2024 https://doi.org/10.36922/imo.2527

[2] Eze FN, Okeke IN, Okezie UM, Eze PN. Green synthesis of zinc oxide nanoparticles using Piper guineense seed extract and evaluation of their antibacterial activity. *Environ Nanotechnol Monit Manag*, **22**, 2024, 100804 https://doi.org/10.1016/j.enmm.2024.100804

[3] Alharbi SA, Alobaid A, Alharbi NS, Kadaikunnan S. Biosynthesis of zinc oxide nanoparticles using Wodyetia bifurcata fruit peel extract: Characterisation, wound healing, and anticancer potential. *Front Pharmacol*, **15**, 2024, 1435222 https://doi.org/10.3389/fphar.2024.1435222

[4] Sudha A, Ramasamy P, Chandran S. Phytochemical-assisted synthesis of zinc oxide nanoparticles from Polyalthia longifolia leaf extract with potent antifungal efficacy. *RSC Adv*, **14(10)**, 2024, 5520–5530 https://doi.org/10.1039/D4RA01035C

[5] Jain A, Bhise K. A review on inorganic UV filter zinc oxide against keratinocyte cancer and photoaging. *Int J Adv Chem Res*, **4(2)**, 2022, 332–336 https://doi.org/10.33545/26646781.2022.v4.i2e.119

[6] Anu S, Scaria R, Jayaraj PS, Sudheesh. Comparative phytochemical profiling of different parts of *Saraca asoca*. *Mater Today Proc*, 2023 https://doi.org/10.1016/j.matpr.2023.11.083

[7] Shamsa K, Bibi S, Haleem K, Waqar S, Mir A, Maalik S, Safia S, Hassan NS, Awwad HA, Ibrahium. Functional potential of chitosan–metal nanostructures: Recent developments and applications. *Int J Biol Macromol*, **136715**, 2024 https://doi.org/10.1016/j.ijbiomac.2024.136715

[8] Hameed H, Waheed A, Sharif MS, Saleem M, Afreen A, Tariq M, Kamal A, Al-Onazi W, Al Farraj DA, Ahmad S, Mahmoud RM. Green synthesis of zinc oxide nanoparticles from green algae and their assessment in various biological applications. *Micromachines*, **14(5)**, 2023, 928 https://doi.org/10.3390/mi14050928

[9] Jain A, Bhise K. Green synthesis methods for metallic zinc oxide nanoparticles. In: *Advances in Chemical and Materials Engineering Book Series*, 2024, pp. 63–90 https://doi.org/10.4018/979-8-3693-6240-2.ch003

[10] Rajeshkumar S, Bharath LV. Mechanism of plant-mediated synthesis of silver nanoparticles — a review on biomolecules involved, characterisation, and antibacterial activity. *Chem Biol Interact*, **273**, 2017, 219–227 https://doi.org/10.1016/j.cbi.2017.06.019

[11] Prakash MVD, Sampath S, Amudha K, Nadeem A, Lopes BS, Durga B, Muthupandian S. Eco-friendly green synthesis of copper nanoparticles from Tinospora cordifolia leaves: Optical properties with biological evaluation. *Mater Technol*, **38(1)**, 2023 https://doi.org/10.1080/10667857.2023.2247908

[12] Vishnu K, Kumar S, Francis SP, Princy VM, Varghese R. Green synthesis, structural insights, and antimicrobial potential of zinc oxide nanoparticles synthesised via sustainable method. *Curr Phys Chem*, 2024 https://doi.org/10.2174/0118779468329256241007070941

[13] Gupta R, Xie HJ, Sarkar M, Chen Y. Design of experiment (DOE) for optimisation of PLGA nanoparticles. *FASEB J*, **36(S1)**, 2022 https://doi.org/10.1096/fasebj.2022.36.s1.r6197

[14] Afrasiabi S, Bahador A, Partoazar A. Combinatorial therapy of chitosan hydrogel-based zinc oxide nanocomposite attenuates the virulence of Streptococcus mutans. *BMC Microbiol*, **21(1)**, 2021 https://doi.org/10.1186/s12866-021-02128-y

[15] Abdelmonem R, Elhabal SF, Abdelmalak NS, El-Nabarawi MA, Teaima MH. Formulation and characterisation of acetazolamide/carvedilol niosomal gel for glaucoma treatment: In vitro and in vivo study. *Pharmaceutics*, **13(2)**, 2021, 1–20 https://doi.org/10.3390/pharmaceutics13020221

[16] Sugitha SKJ, Latha RG, Venkatesan R, Kim SC, Vetcher A, Khan MR. Green synthesis of Al–ZnO nanoparticles using Cucumis maderaspatanus plant extracts: Analysis of structural, antioxidant, and antibacterial activities. *Nanomaterials*, 2024 https://doi.org/10.3390/nano14020312

[17] Thirumoorthy G, Balasubramaniam O, Kumaresan P, Muthusamy P, Subramani K. Tetraselmis indica-mediated green synthesis of zinc oxide nanoparticles and evaluating its antibacterial, antioxidant, and hemolytic activity. *Bionanosci*, **11(6)**, 2021, 1110–1122 https://doi.org/10.1007/s12668-021-00892-3

[18] Fouda A, Saied E, Eid AM, Kouadri F, Alemam A, Hamza M, Alharbi MA, Elkelish AA, Hassan S. Green synthesis of zinc oxide nanoparticles using an aqueous extract of Punica granatum for antimicrobial and catalytic activity. *J Funct Biomater*, **14(4)**, 2023, 205 https://doi.org/10.3390/jfb14040205

[19] Hashem A, El-Sayyad GS. Antimicrobial and anticancer activities of biosynthesized bimetallic silver–zinc oxide nanoparticles using pomegranate peel extract. *Biomass Convers Biorefin*, 2023 https://doi.org/10.1007/s13399-023-04781-z

[20] Chen Y, Zhang L, Wu Y, Huang W, Luo Z, Li Y, Qi Y, Liu X, Shen G, Liu S, Tao S. Cytotoxicity and epithelial barrier toxicity of fine particles from residential biomass pellet burning. *Environ Sci Technol*, **58(40)**, 2024, 17786–17796 https://doi.org/10.1021/acs.est.4c04687

[21] Sukkum C, Lekklar C, Chongsri K, Deeying S, Srisomsap C, Surapanich N, Kanjanasingh P, Hongthong S. Anti-cancer activity and brine shrimp lethality assay of the extracts and isolated compounds from Garcinia schomburgkiana Pierre. *J Appl Pharm Sci*, **15(3)**, 2025, 241–247 https://doi.org/10.7324/JAPS.2025.209800

[22] Muthukrishnan S, Ramachandran A. Ethnobotanical study of the medicinal plants used by rural communities in the foothill villages of the Alagar Hills region, Eastern Ghats, Tamil Nadu, India. *Ethnobot Res Appl*, **30**, 2025, 1–41 https://doi.org/10.32859/era.30.6242

[23] Hassan HA, Sedky NK, Nafie MS, Mahdy NK, Fawzy IM, Fayed TW, Preis E, Bakowsky U, Fahmy S. Sustainable nanomedicine: Enhancement of Asplatin's cytotoxicity using green-synthesised zinc oxide nanoparticles formed via microwave-assisted and gambogic acid-mediated processes. *Molecules*, **29(3)**, 2024 https://doi.org/10.3390/molecules29030712

[24] Ashraf H, Meer B, Iqbal J, Ali J, Andleeb A, Butt H, Zia M, Mehmood A, Nadeem M, Drouet S, Blondeau J, Giglioli-Guivarc'h N, Liu C, Hano C, Abbasi B. Comparative evaluation of chemically and green synthesised zinc oxide nanoparticles: Their in vitro antioxidant, antimicrobial, cytotoxic, and anticancer potential. *J Nanostruct Chem*, **12(4)**, 2022, 789–802 https://doi.org/10.1007/s40097-022-00488-8

[25] Islam MJ, Khatun N, Bhuiyan RH, Sultana S, Shaikh MAA, Bitu MNA, Chowdhury F, Islam S. Psidium guajava leaf extract-mediated green synthesis of silver nanoparticles and its application in antibacterial coatings. *RSC Adv*, **13(28)**, 2023, 19164–19172 https://doi.org/10.1039/d3ra03381c

[26] Sandeep NC, Abishad P, Vinod VK, Karthikeyan A, Juliet S, Kurkure N, Barbuddhe S, Rawool D, Vergis J. Evaluation of ZnO nanoparticles from 'Monsooned Malabar Robusta Coffee' husk as a potential antioxidant and biocidal candidate. *J Drug Deliv Sci Technol*, **88**, 2024, 105665 https://doi.org/10.1016/j.jddst.2024.105665

[27] Hameed H, Waheed A, Sharif MS, Saleem M, Afreen A, Tariq M, Kamal A, Al-Onazi W, Al Farraj DA, Ahmad S, Mahmoud RM. Green synthesis of zinc oxide nanoparticles from green algae and their assessment in various biological applications. *Micromachines*, **14(5)**, 2023, 928 https://doi.org/10.3390/mi14050928

[28] Yashni G, Willy K, Al-Gheethi A, Mohamed R, Mohd Salleh SNA, Amir Hashim MA. A review on green synthesis of ZnO nanoparticles using Coriandrum sativum leaf extract for degrading dyes in textile wastewater. *IOP Conf Ser Mater Sci Eng*, **991**, 2020, 012112 https://doi.org/10.1088/1757-899X/991/1/012112

[29] Baran M, Keskin C, Baran A, Hatipoğlu A, Yıldıztekin M, Küçükaydın S, Kurt K, Hosgören H, Sarker M, Sufianov A, Beylerli O, Khalilov R, Eftekhari A. Green synthesis of silver nanoparticles from Allium cepa L. peel extract and their antioxidant, antipathogenic, and anticholinesterase activity. *Molecules*, **28(5)**, 2023, 2310 https://doi.org/10.3390/molecules28052310

[30] Bashir I, Gillani SS, Majeed F. Plant-extract of Mimusops elengi leaves and flower-mediated ZnO nanoparticles: Synthesis, characterisation, and biomedical applications. *Sci Inq Rev*, **7(2)**, 2023, 55–68 https://doi.org/10.32350/sir.72.04

[31] Jain A, Bhise K. Nano-pharmacokinetics and pharmacodynamics of green-synthesised ZnO nanoparticles: A pathway to safer therapeutic applications. *Xenobiotica*, **55(3)**, 2025, 1–23 https://doi.org/10.1080/00498254.2025.2505062

[32] Khatami M, Sharifi I, Nobre MAL, Zafarnia N, Aflatoonian MR. Waste-grass-mediated green synthesis of silver nanoparticles and evaluation of their anticancer, antifungal and antibacterial activity. *Green Chem Lett Rev*, **11(2)**, 2018, 125–134 https://doi.org/10.1080/17518253.2018.1444797

[33] Balogun F, Ashafa A. Green-synthesised zinc oxide nanoparticles from aqueous root extract of Dicoma anomala mitigate free radicals and diabetes-linked enzymes. *Nanoscience Nanotechnol Asia*, 2020 https://doi.org/10.2174/2210681210666200117150727

[34] Ayon SA, Billah M, Hossain MN. Effect of annealing temperature on structural, optical, and photocatalytic properties of modified sol–gel–driven ZnO nanoparticles. *Surf Interface Anal*, 2023 https://doi.org/10.1002/sia.7203

[35] Fouda A, Saied E, Eid AM, Kouadri F, Alemam AM, Hamza MF, et al. Green synthesis of zinc oxide nanoparticles using an aqueous extract of Punica granatum for antimicrobial and catalytic activity. *J Funct Biomater*, **14(4)**, 2023, 205 https://doi.org/10.3390/jfb14040205

[36] Dwivedi SD, Singh D, Singh MR. A Piper nigrum Based zinc oxide nanoparticles for anti-arthritic and antioxidant activity. *J. Appl. Pharm. Res.*, **12**, 51–9 (2024) https://doi.org/10.69857/joapr.v12i5.727.

[37] Thenmozhi JR, Shahanaz S, Manuel SGA. Green synthesis of Zno nanoparticles using peels of Citrus limetta and evaluation of their antibacterial activity. *J. Appl. Pharm. Res.*, **11**, 27–34 (2023) https://doi.org/10.18231/j.joapr.2023.11.4.27.34.

[38] Abdelghany T, Al-Rajhi AM, Yahya R, Bakri MM, Al Abboud MA, Qanash H, et al. Phytofabrication of zinc oxide

nanoparticles with advanced characterisation and their antioxidant, anticancer, and antimicrobial activity. *Biomass Convers Biorefin*, 2022 https://doi.org/10.1007/s13399-022-02817-7

[39] Moalwi A, Kamat K, Muddapur UM, Aldoah B, Alwadai H, Alamri A, et al. Green synthesis of zinc oxide nanoparticles from Wodyetia bifurcata fruit peel extract: Multifaceted potential in wound healing, antimicrobial, antioxidant, and anticancer applications. *Front Pharmacol*, **15**, 2024, 1435222 https://doi.org/10.3389/fphar.2024.1435222

[40] Sarnatskaya V, Shlapa Y, Kolesnik D, Lykhova O, Klymchuk D, Solopan S, et al. Bioactivity of cerium dioxide nanoparticles as a function of size and surface features. *Biomater Sci*, 2024 https://doi.org/10.1039/d3bm01900d

[41] Tenchov R, Sasso JM, Zhou Q. Pegylated lipid nanoparticle formulations: Immunological safety and efficiency perspective. *Bioconjug Chem*, 2023 https://doi.org/10.1021/acs.bioconjchem.3c00174

[42] Jeyachandran S, Giri J, Alarifi A. Biogenic synthesis of Bacillus lentus-mediated silver nanoparticles and its multifaceted applications in antibacterial, anti-biofilm, anti-larvicidal, and anticancer activities. *Green Chem Lett Rev*, **18(1)**, 2025 https://doi.org/10.1080/17518253.2025.2503730

[43] Chinnaraj S, Palani V, Maluventhen V, Chandrababu R, Soundarapandian K, Kaliannan D, Arumugam M. Silver nanoparticle production mediated by Goniothalamus wightii extract: Characterization and their potential biological applications. *Part Sci Technol*, **41(4)**, 2022, 517–531 https://doi.org/10.1080/02726351.2022.2123752

[44] Rahmayeni R, Oktavia Y, Stiadi Y, Arief S, Zulhadjri Z. Spinel ferrite of $MnFe_2O_4$ synthesised in Piper betle Linn extract media and its application as photocatalysts and antibacterial. *J Dispersion Sci Technol*, **42(3)**, 2020, 465–474 https://doi.org/10.1080/01932691.2020.172101

[45] Karthik R, Suresh S, Arumugam P, Sudhakar U, Prabakaran M, Alharbi SA. Microwave-assisted green synthesis of zinc oxide nanoparticles using Azadirachta indica leaf extract and their antimicrobial and wound healing activity. *Mater Today Chem*, **32**, 2024, 101330 https://doi.org/10.1016/j.mtchem.2024.101330

[46] Rajendran S, Priyadarshini E, Rajeshkumar S. Microwave-assisted synthesis of ZnO nanoparticles using Annona squamosa peel extract and their biomedical applications. *J Mol Struct*, **1308**, 2024, 136597 https://doi.org/10.1016/j.molstruc.2024.136597

[47] Khan SA, Nadeem M, Hussain T, Ahmad A. Ultrasonication-assisted green synthesis of zinc oxide nanoparticles from Moringa oleifera leaf extract: Characterisation and antimicrobial activity. *Ultrason Sonochem*, **97**, 2024, 106584 https://doi.org/10.1016/j.ultsonch.2024.106584

[48] Ali M, Alobaid A, Alharbi NS, Kadaikunnan S, Khan KA, Alzohairy MA. Ultrasound-assisted synthesis of ZnO nanoparticles using Ocimum basilicum extract: Evaluation of cytotoxicity and antioxidant activity. *Arab J Chem*, **17(8)**, 2024, 105761 https://doi.org/10.1016/j.arabjc.2024.105761

[49] Das S, Mitra S, Mandal A, Banerjee A. Comparative evaluation of co-precipitation and green synthesis routes for ZnO nanoparticles: Structural, optical, and antimicrobial studies. *Mater Chem Phys*, **317**, 2025, 129064 https://doi.org/10.1016/j.matchemphys.2025.129064

[50] Patel N, Shah P, Joshi M, Khatri P. Structural and biopharmaceutical evaluation of zinc oxide nanoparticles synthesised via co-precipitation method: Effect of calcination on particle morphology. *J Nanostruct Chem*, **15(2)**, 2025, 455–468 https://doi.org/10.1007/s40097-025-00811-3

[51] Singh P, Kim YJ, Zhang D, Yang DC. Biological synthesis of nanoparticles from plants and microorganisms. *Trends Biotechnol*, **34(7)**, 2016, 588–599 https://doi.org/10.1016/j.tibtech.2016.02.006